Tortuosity and mass transfer limitations in industrial hydrotreating catalysts: effect of particle shape and size distribution

Svetan Kolitcheff, Elsa Jolimaître, Antoine Hugon, Jan Verstraete, Mickael Rivallan, Pierre-Louis Carrette, Françoise Couenne, Mélaz Tayakout-Fayolle

▶ **To cite this version:**

Svetan Kolitcheff, Elsa Jolimaître, Antoine Hugon, Jan Verstraete, Mickael Rivallan, et al.. Tortuosity and mass transfer limitations in industrial hydrotreating catalysts: effect of particle shape and size distribution. Catalysis Science & Technology, 2018, 8 (17), pp.4537 - 4549. 10.1039/C8CY00831K . hal-01912119

HAL Id: hal-01912119
https://ifp.hal.science/hal-01912119

Submitted on 5 Nov 2018

HAL is a multi-disciplinary open access archive for the deposit and dissemination of scientific research documents, whether they are published or not. The documents may come from teaching and research institutions in France or abroad, or from public or private research centers.

L'archive ouverte pluridisciplinaire **HAL**, est destinée au dépôt et à la diffusion de documents scientifiques de niveau recherche, publiés ou non, émanant des établissements d'enseignement et de recherche français ou étrangers, des laboratoires publics ou privés.

TORTUOSITY AND MASS TRANSFER LIMITATIONS IN INDUSTRIAL HYDROTREATING CATALYSTS: A MULTITECHNIQUE STUDY

Svetan Kolitcheff[1], Elsa Jolimaitre[1*], Antoine Hugon[1], Jan Verstraete[1], M. Rivallan[1], Pierre-Louis Carrette[1], Françoise Couenne[2], Mélaz Tayakout-Fayolle[2]

[1] IFP Énergies nouvelles, Rond-point de l'échangeur de Solaize – BP 3 – 69360 Solaize, France

[2] Laboratoire d'Automatique et de Génie des Procédés, UMR 5007, CNRS-ESCPE 43 Bd du 11 Novembre 1918, 69622 Villeurbanne, France

[*] Corresponding author

Abstract

The tortuosity factor of γ-alumina supports and catalysts used in hydrotreating applications was evaluated in liquid phase with three different techniques: Pulse Field Gradient-NMR (PFG-NMR), Inverse Liquid Chromatography (ILC) and catalytic experiments in a batch reactor. In order to satisfy the specific experimental constraints associated to each technique, tortuosity factor values were evaluated in a wide range of operating conditions: temperature was varied from 25°C to 340°C, catalyst particles were used as-synthesized (trilobe extrudates) or crushed, the liquid composition was either pure toluene, n-heptane/squalane mixtures, or squalane/2,5-bis-(octadecyl)thiophene mixtures. It is demonstrated that not taking into account both the shape factor and the size distribution of the particles can lead to significant errors on the tortuosity factor value. For both parameters, the optimal mean spherical radius depends on the contribution of internal diffusion to the overall performance. When internal diffusion is the limiting step, a new expression for the mean radius of distributed particle is proposed and validated by comparison between ILC and PFG-NMR results. This expression is transposable to any catalytic system, making it possible to measure tortuosity factors using either microscopic or macroscopic methodologies. Moreover, the tortuosity factors obtained with ILC and NMR are in good agreement with the one estimated from the catalytic experiments, showing that mass transfer parameters can be extrapolated from non-reactive to reactive conditions.

Introduction

Hydrotreating of petroleum or biomass feedstocks are heterogeneously catalysed processes whose purpose is to purify the feeds from unwanted sulphur, nitrogen, oxygen and/or unsaturated compounds. Industrial hydrotreating catalysts are composed of a sulphide active phase, usually Mo sulphide (more rarely W sulphide) doped with Ni or Co and supported on a high surface oxide, in most cases γ-alumina[1].

While the optimization of the sulphide active phase has been the subject of numerous studies[1], the effect of mass transfer properties on the final catalyst performances has been far less documented. Yet, both the chemical kinetics and mass transfer rates are required to optimize the catalyst formulation, and ultimately the process operating conditions. Simple and reliable experimental methods to evaluate the effective diffusion coefficients in hydrotreating catalysts would therefore be very useful.

For high boiling vacuum residue fractions (boiling point > 550°C), which contain very voluminous molecules such as asphaltenes, diffusion is hindered by friction of the molecules with the pore walls. The effective diffusion coefficients therefore depend not only on the pore network of the catalyst, but also on the size of the diffusing molecules. For lower boiling petroleum cuts (boiling point < 550°C), such as vacuum distillates or atmospheric gas oils, the diffusion regime is molecular[2] and the effective diffusion coefficient inside the catalyst can be evaluated using the following expression:

$$D_{eff} = \frac{D_m}{\tau} \quad (1)$$

where D_m is the molecular diffusion coefficient, which can be measured or estimated using existing correlations, and τ the tortuosity factor of the catalyst. As can be noticed, in the molecular diffusion regime, the tortuosity factor is independent of the diffusing molecule.

To estimate the tortuosity factor of a given catalyst, a first possibility is to rely on correlations proposed in the literature[3]. Indeed, the relation between tortuosity and porosity in porous systems has been extensively studied. Various equations have been proposed in the literature[3] depending for example on the morphology and size distribution of the stacked particles. However, as shown in a previous paper[2], these correlations are not valid for hydrotreating γ-alumina supports, because of the multi-scale organization of their pore networks.

For such complex porous structures, it is therefore necessary to determine the tortuosity factor using experimental techniques. As previously mentioned, when the diffusion regime is molecular, the tortuosity factor τ is independent of the properties of the diffusing molecule. In theory, it is hence possible to measure this parameter at experimental conditions (i.e. temperature, pressure, diffusing molecules) that differ from those of the actual catalytic process, as long as the molecular diffusion regime is maintained. This opens gateways to a whole set of experimental techniques. The details of the available techniques to measure effective diffusion coefficients have been reviewed elsewhere[4]. They can be divided into two main categories:

- Microscopic techniques, which probe diffusion over small distances (i.e. up to a few micrometres)
- Macroscopic techniques, which take into account the mass limitations over the whole catalyst pellet, including mass transfer from the fluid phase to the surface of the solid.

The first aim of this work is to measure the tortuosity factor of γ-alumina pellets using both types of techniques. Unless the pore network contains long range heterogeneities, such as diffusion barriers or cracks in the pellets, methods from the two categories are expected to give the same results. Pulse Field Gradient-NMR (PFG-NMR) and Inverse Liquid Chromatography (ILC) were selected as the microscopic and macroscopic techniques, respectively. Secondly, hydrodesulphurization kinetics was

acquired in a batch reactor with pellets of different sizes, so as to evaluate the extrapolability of the measured tortuosity factors values under reactive conditions.

The pros and cons, as well as the experimental conditions applied in this work for each technique, are briefly listed in Table 1. Once the pulse sequence has been implemented and validated, PFG-NMR is by far the easiest and fastest technique. Only a few minutes are needed to acquire the signal and no additional textural characterizations are needed. However, the experimental conditions are very different from those occurring in a hydrotreating reactor. ILC can be operated at higher temperature and higher pressure, but its drawback is the complexity of the experimental procedure. Moreover, the tortuosity factor calculated from ILC experiments is dependent on the porosity, shape and size of the pellets, values that are not always easy to acquire with adequate precision.

It is also clear from Table 1 that none of these two techniques is really close to the operating conditions of the hydrotreating reactor. In addition to the differences in pressure and temperature, one has to keep in mind all factors that differ: feed composition, hydrodynamics of the reactor, gas phase injection of hydrogen, presence of the sulphide active phase in the pore network, possible pore blocking due to coke deposition… The aim of this paper is therefore to evaluate to what extent the tortuosity factor of heterogeneous catalysts can be evaluated under non-reactive conditions.

	PFG-NMR	**ILC**	**Catalytic reactor**
Diffusion mechanism	self-diffusion	transport diffusion	transport diffusion
Pros	• Small quantity of solid • Fast • Size of the particles not needed	• Possibility to work at high temperature and high pressure	• Operating conditions close to industrial conditions
Cons	• Low temperature • Low pressure	• Min. 10 g of solid • Difficult to differentiate between external and internal diffusion • Catalyst porosity and mean pellet radius have to be known	• Long and complex experiments • Difficult to differentiate external/internal diffusion and chemical kinetics • Catalyst porosity and mean pellet radius have to be known
Experimental conditions used in this work			
Temperature (°C)	25	35	340
Pressure (bar)	1	1	56
Fluid composition	• Toluene	• Squalane (SQ) • n-heptane (nC7)	• Squalane (SQ) • 2,5-bis-(octadecyl)thiophene ($C_{40}H_{76}S$) • H_2

Table 1: Comparison of different experimental methods to evaluate the tortuosity of a catalyst support

Experiments and Methods

Alumina supports synthesis

Five γ-alumina supports, provided by IFPEN, were studied in this work. The γ-alumina supports, referenced A to E, are obtained by precipitation of aluminium salts in an aqueous solution. The boehmite precipitate was filtered and washed. Shaping involves the passage from a boehmite powder to support pellets. The extrudates are trilobes. Their diameter ranges from 1.2 to 2 mm and their length from 2 to 6 mm. A thermal treatment at high temperature (from 798 to 1248 K) was performed to obtain the final support. The aim of these thermal treatments is to optimize the particle size, which increases with temperature, the average pore diameter, the total pore volume, and the surface area. The final γ-alumina supports have a purity >99% by weight. The added impurities, introduced during the precipitation in the aqueous solution, are P, Na, Cl and Mg elements. These impurity quantities do not have any effect on textural properties.

Catalyst preparation

The NiMoP/Al_2O_3-supported catalyst was prepared by incipient wetness impregnation of the γ-alumina support D (Table 2), with an aqueous solution containing MoO_3 (purity 100%), $Ni(OH)_2$ (purity 99.5%), and H_3PO_4 (purity 85%) so as to reach 18% weight percent of MoO_3 and Ni/Mo and P/Mo molar ratios of 0.4. Following the impregnation step, the solid was matured in a saturated water atmosphere during 12 h in order to ensure a good diffusion of the precursors into the alumina porosity. Then, a drying step at 393 K overnight in a static air oven was carried out to obtain the dried NiMoP sample. After the drying step, the catalyst was calcined under air flow (1 L/h/g_{solid}) by heating the sample up to 723 K for 4 h with a heating ramp of 5 K/min. The calcined NiMoP oxidic sample thus obtained will be referenced hereafter as “catalyst CD”. Its metal content was determined by X-ray fluorescence (17.2 wt % MoO_3, 4.4 wt % NiO and 3.2 wt% P_2O_5). Catalyst CD was further sulphided by raising the temperature at a rate of 5 K/min from room temperature to 623 K under a flow of a mixture of 15% of H_2S into H_2 at atmospheric pressure (2 L/h/$g_{catalyst}$). After reaching 623 K, the catalyst was maintained under a sulphiding atmosphere for 4 h. The sulphided catalyst will be referenced hereafter as “catalyst SCD”.

Textural properties

The textural properties were measured by physical nitrogen adsorption on the ASAP 2420 instrument and helium pycnometry on the Accupyc 1340 instrument, after pre-treatment at 350°C for 3 hours under vacuum.

The BET surface area S_{BET} and the pore volume V_p, obtained with the t-plot method, were evaluated from the nitrogen isotherm. Helium pycnometry provided the structural density ρ_s. The particle porosity ε_p of all studied solids was calculated by means of the following equation:

$$\varepsilon_p = \frac{V_p}{V_p + \frac{1}{\rho_s}} \qquad (2)$$

The textural properties of all alumina supports are reported in Table 2.

Alumina support	S_{BET} ($m^2.g^{-1}$)	V_p ($cm^3.g^{-1}$)	ρ_s ($g.cm^{-3}$)	ε_p
A	340	0.71	3.3	0.72
B	300	0.72	3.3	0.70
C	290	0.78	3.3	0.72
D	270	0.74	3.3	0.71
E	160	0.77	3.5	0.73
CD	200	0.49	3.7	0.64

Table 2: Alumina supports textural properties (CD: catalyst based on support D)

The values of the pore volume, porosity and structural density are very close for all samples. Only the BET surface area S_{BET} varies significantly, meaning that the elementary building blocks generated during the particle synthesis display different surface/volume ratios.

The BJH method was used to estimate the pore size distributions of the studied alumina supports from the nitrogen desorption branch, which are reported in Figure 1(b).

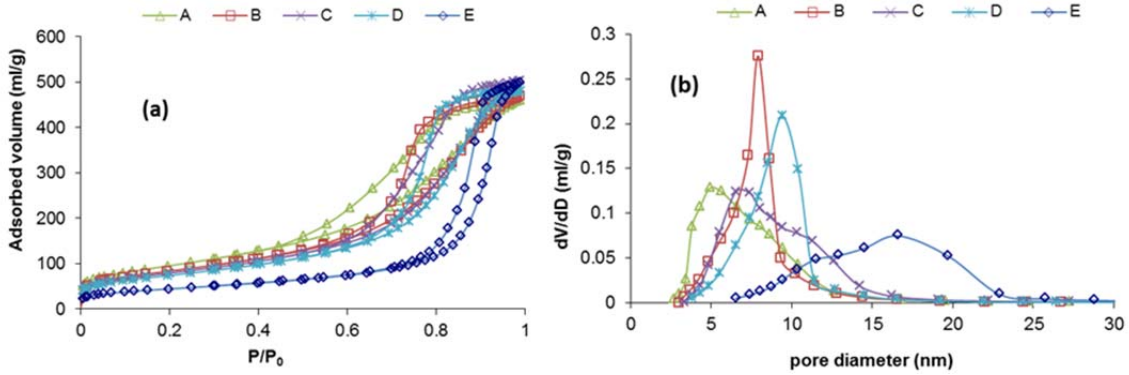

Figure 1: (a) Nitrogen isotherms for the alumina supports; (b) Pore size distribution estimated by means of the BJH method for the alumina supports

The studied aluminas are mainly mesoporous: no microporosity is observed by physical nitrogen adsorption, while the Hg intrusion does not show any macroporosity. The pore size distributions of the different samples vary significantly. Aluminas B and D seem to be almost mono-disperse while the three others are at least bimodal. Besides this, the maximum in the pore size distribution increases from A to E, with a value of about 5 nm for sample A and nearly 17 nm for sample E.

The effect of the impregnation of γ-alumina support D with the metal oxides is illustrated in Figure 2 and quantified in Table 2. The impregnated oxide layer causes a large reduction of the BET surface area S_{BET} and pore volume V_p, but the high density of the added oxide phase is partly accountable for this effect (since S_{BET} and V_p are evaluated for a given catalyst mass). Indeed, the variation of ε_p, i.e. the pore volume expressed per unit volume of catalyst, is only of the order of 10%. It can be seen in Figure 2 that, when the volume adsorbed is expressed per unit volume of catalyst, the difference

between the adsorption isotherms is relatively small, particularly for $P/P_0 < 0.6$. Still, pores with a diameter higher than 10 nm are slightly impacted by the impregnation step.

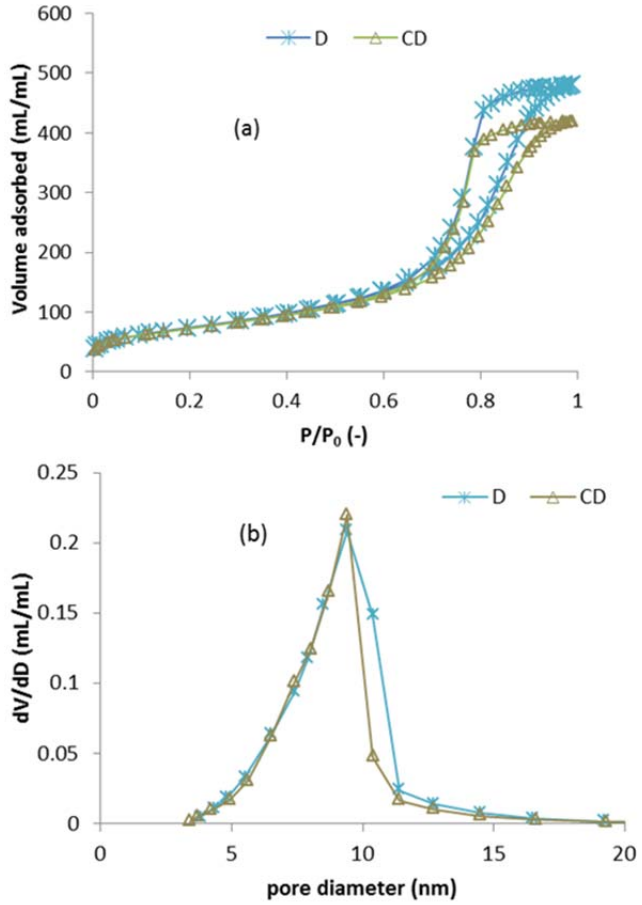

Figure 2: (a) Nitrogen isotherms of support D and catalyst CD; (b) Corresponding pore size distribution estimated by means of the BJH desorption method

Determination of the equivalent and mean particle radii

Industrial hydrotreating catalyst supports are generally produced by extrusion. The extrudates can be shaped in different forms, depending on its application and on the catalyst vendor: cylinders, trilobes, quadrilobes, etc.

While the size and shape of the particle is not an issue for PFG-NMR measurements (because the measurement time is selected such that only the porosity inside the pellets is probed by the molecules), for ILC and for catalytic experiments, however, the size and shape of the catalyst have to be evaluated with precision. Indeed, for both techniques, what is measured is the evolution of the fluid phase concentration over time, from which – using a model of the process – characteristic diffusion times can be estimated. These characteristic diffusion times represent the time necessary for a molecule to reach the centre of the catalyst, and are therefore intrinsically dependent of the size and shape of the particle (the exact expression of this parameter will be discussed in the next

sections). Moreover, the models generally used to interpret these experiments are based on the assumption of a Fickian diffusion inside a sphere, meaning that for non-spherical particles, an equivalent-sphere radius has to be calculated.

In this paper, supports of different sizes and shapes are used. For ILC experiments, the trilobe supports were crushed and sieved, so as to ensure a controlled fluid phase hydrodynamic profile in the columns. For the catalytic experiments, both as-synthesized and crushed trilobes were tested, in order to differentiate between mass transfer and intrinsic chemical kinetics. The calculation of the mean radius is specific for these two types of particles:

- for trilobe pellets, whose actual shape is quite complicated, one has to find the correct expression of the equivalent spherical radius;
- for crushed particles, which are distributed in size, it is necessary to appropriately calculate the mean particle radius.

Calculation of the mean radius of crushed particles

For ILC and some of the catalytic experiments, aluminas and catalysts were crushed and sieved in different size fractions. In order to evaluate their morphology, pictures of crushed and sieved samples have been acquired with an optical microscope (Figure 3).

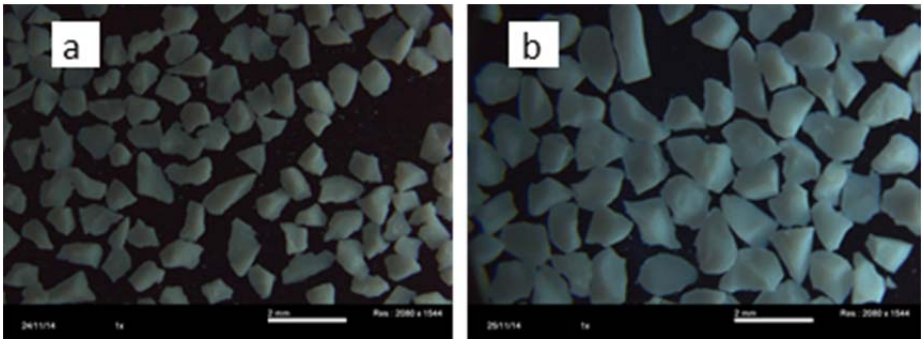

Figure 3: Morphology of crushed particles: (a) sieved between 500-630 μm; (b) sieved between 800-900 μm

The particles are irregular in shape. To assess their particle size, classic granulometric techniques were used, even though this generally implies that the particles are assumed to behave as spherical particles. The particle sizes were measured by laser granulometry by means of a Malvern Mastersizer 3000. The solids were suspended in nitrogen. The diffraction pattern was used to estimate the size of the particles using the Fraunhofer theory. The resulting radius distributions for sample D are reported in Figure 4.

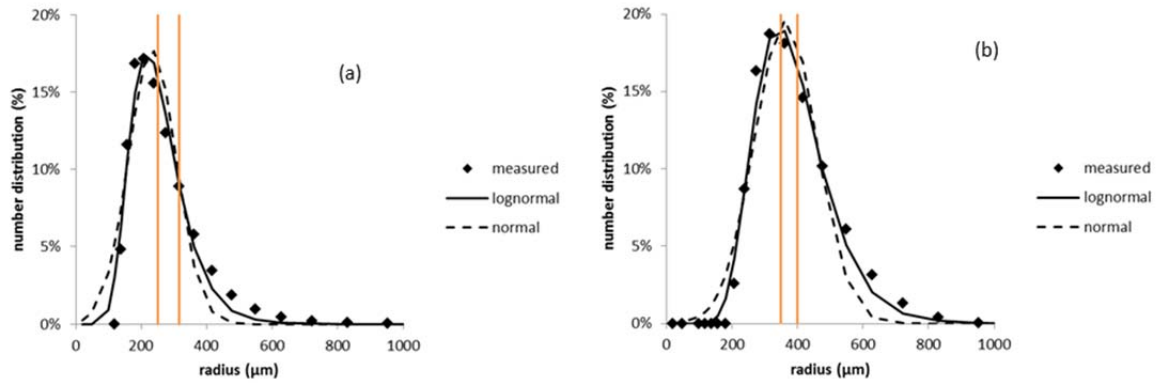

Figure 4: Radius distribution in number for crushed particles (sample D): (a) sieved between mesh sizes of 500-630 μm; (b) sieved between mesh sizes of 800-900 μm (orange lines: theoretical minimal and maximal radii given by the mesh size of the sieves)

The particle radii are highly dispersed. A large number of particles have a radius outside the limits defined by the size of the sieves (represented by orange lines in Figure 4). This is due to the anisotropy of the crushed particles, which can pass or be blocked by the sieving meshes depending on their orientation. As can be seen in Figure 4, the particle size distribution is non-symmetrical and can therefore not be represented as a Gaussian distribution. A lognormal distribution function seems to be more suited. Given the high dispersion of the distribution curves, the calculation of the mean radius of the particles has therefore to be carried out based on appropriate hypotheses.

While size-distributed particles are frequent in labs and industry, articles dealing with the influence of size distribution on intraparticle diffusion are not so common in the literature. Using simulation tools, it has been demonstrated that the particle size distribution has quite some influence on experimental results for thermogravimetric[5,6], batch[7,8], and chromatographic[9-14] systems. Moreover, the effect is more pronounced for asymmetric distributions[10,11,13-15], as is the case for our particles.

Inserting the exact size distribution function into the mass transfer model significantly complicates the equations. It is therefore very common to substitute the size distribution function with a unique mean particle radius. Different mean radii have been defined depending on the physicochemical phenomena under study. For mass transfer applications, the Sauter mean radius $\bar{R}_S$ and the mean square radius $\bar{R}_{ms}$ (see Table 3) are the most commonly used.[8,13]. Hayot et al.[13] showed that the mean square radius $\bar{R}_{ms}$ enables a better fit of the concentration profiles than the Sauter mean radius $\bar{R}_S$ under high internal mass transfer limitations. Fong et al.[12] have simulated breakthrough curves under different conditions and concluded that the choice of the "best" radius depends on the part of the curve (short time region or long time region) one focuses on. In this study, another mean radius is introduced, based on mean molar intraparticle flux density calculations (see calculation details in the ESI).

Name	Definition	Criterion
Sauter Mean Radius	$\bar{R}_S = \frac{\sum_i x_i . {R_i}^3}{\sum_i x_i . {R_i}^2}$	Same surface/volume
Mean Square Radius	$\bar{R}_{ms} = \sqrt{\sum_i x_i . {R_i}^2}$	Same dispersion (second moment) of the breakthrough curve
Mean Molar Flux Radius	$\bar{R}_{mmf} = \sqrt{\sum_i \frac{x_i \cdot R_i^3}{x_i \cdot R_i}}$	Same mean molar flux density (see ESI)

Table 3: Definition of different mean radii (with x_i the number fraction of radius R_i)

The values of the different mean radii for all alumina samples are given in Table 4.

Sample	Sieves opening min-max (μm)	$\bar{R}_S$ (mm)	$\bar{R}_{ms}$ (mm)	$\bar{R}_{mmf}$ (mm)
A	700-800	0.498	0.399	0.461
B	700-800	0.498	0.394	0.459

C	700-800	0.486	0.382	0.446
D	500-630	0.328	0.262	0.303
D	700-800	0.442	0.387	0.422
E	700-800	0.457	0.373	0.426

Table 4: Calculated mean radii for the different alumina samples

The radii are compatible with the range of the sieves and rank in the following order: $\bar{R}_{ms}$<$\bar{R}_{mmf}$<$\bar{R}_S$. The difference between $\bar{R}_{ms}$ and $\bar{R}_S$ is significant, and varies between 14% and 27% depending on the sample. Hence, the choice and the influence of the mean radius on the tortuosity factor values obtained by ILC will need to be taken into account (see Results and Discussion section).

Evaluation of the sphere-equivalent radius for a trilobe extrudate

The trilobe extrudates are manually sorted by length (4-5 mm) before the catalytic experiments and are therefore fairly homogeneous in size. In the same manner as for the crushed particles, two sphere-equivalent diameters have been calculated. The calculation steps and main hypotheses are schematically depicted in Figure 5.

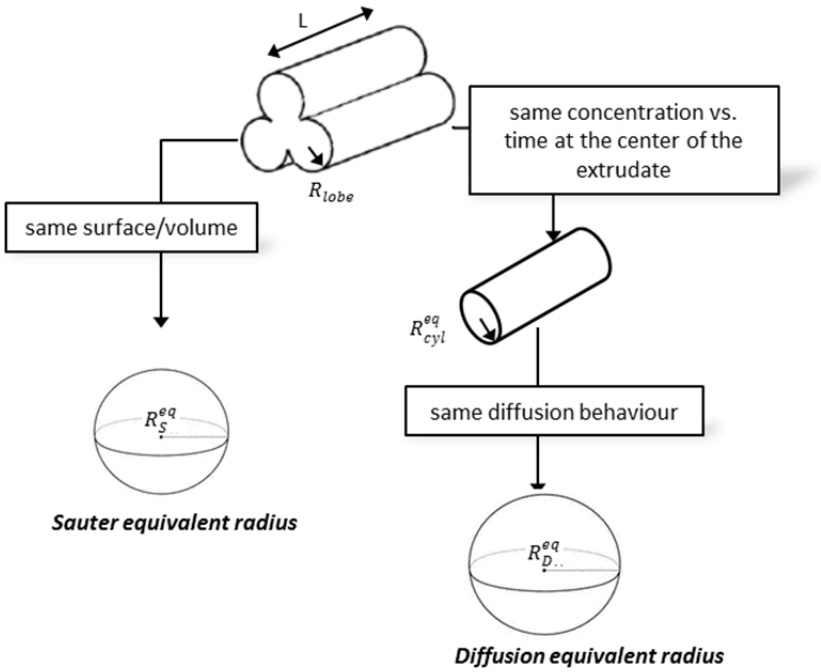

Figure 5: Calculation steps for the sphere-equivalent diameters of trilobe extrudates

The Sauter-equivalent radius R_S^{eq} (i.e. the radius that maintains the surface/volume ratio) has been calculated in the work of Ancheyta et al.,[16] who evaluated the surface and the volume of trilobe extrudates depending on their length and on the lobe radius. The Sauter-equivalent radius R_S^{eq} is quite straightforward to calculate.

Calculation of the diffusion-equivalent radius R_D^{eq} requires two steps. First, the cylinder-equivalent radius is evaluated based on the simulations of Mesmier et al.,[17] who compared the concentration profiles inside trilobes and cylinders. The cylinder-equivalent radius R_{cyl}^{eq} that best fits the concentration profile over time at the centre of the trilobe pellet is approximately equal to

$1.53 \cdot R_{lobe}$. Next, the shape factors proposed by van Genuchten[18] to maintain the same diffusion properties between a finite length cylinder and a sphere were applied.

Mean length L (mm)	4.5
Lobe radius R_{lobe} (mm)	0.58
Surface/volume[16] (m^{-1})	3.58
R_{cyl}^{eq} [17] (mm)	0.88
R_{S}^{eq} [16] (mm)	0.84
R_{D}^{eq} (mm)	1.14

Table 5: Size and equivalent diameters for trilobes (definitions of the variables shown in Figure 5)

The length and equivalent radii obtained with the two procedures are given in Table 5. As can be seen, the two equivalent radii calculated using different assumptions vary significantly (>20%). The best choice for the radius will be further discussed in the Results and Discussion section.

PFG-NMR experiments

PFG-NMR experiments have been performed as described by Wang et al.[19]. A single extrudate is placed in a 5 mm diameter tube and immersed in 10% deuterated toluene. The deuterated fraction has the purpose of locking the NMR probe on the deuterium resonance frequency. Measurements were performed with a Bruker Avance 600 spectrometer (600 MHz resonance frequency for proton). During the experiments, the temperature is controlled at 295 K. The echo attenuation coefficients are measured using stimulated echo sequences with parameters δ = 2.5 ms, Δ = 140 ms and τ = 0.05 µs. q -Space is probed by varying the intensity of the gradient g (from 6.81 x 10^{-3} T.m-1 to 3.24 x 10^{-1} $T.m^{-1}$), in order to obtain 64 values of attenuation ranging from 2 to 95%. The data are processed by the software "Dynamics Center 2.3.1" from Bruker[20]. Molecular diffusion of free toluene is measured independently using the same experimental procedure, yielding D_m=2.4 10^{-9} m^2/s at 295 K. As the molecules are tracked over very short distances, the tortuosity factor can be calculated from equation (2):

$$\tau = \frac{D_m}{D_{eff}} \qquad (2)$$

Molecular diffusion of liquid binary mixtures (1 vol.% squalane in nC_7, and 1 vol.% 2,5-bis-(octadecyl)thiophene in squalane), required to interpret the ILC and catalytic experiments, have been measured using the same NMR probe and spectrometer at 308 K. An internal capillary (1.7 mm diameter) containing $CDCl_3$ as reference has been used. The echo attenuation coefficients are measured using stimulated echo sequences with parameters δ = 2.5 ms, τ = 0.05 µs, and Δ = 140 ms or 500 ms for the nC_7 or squalane solvent, respectively. The observation time is longer for squalane, due its lower molecular diffusion coefficient.

Inverse Liquid Chromatography experiments

The ILC experiments were described in detail in a previous paper[2]. The experimental setup is schematically represented in Figure 6.

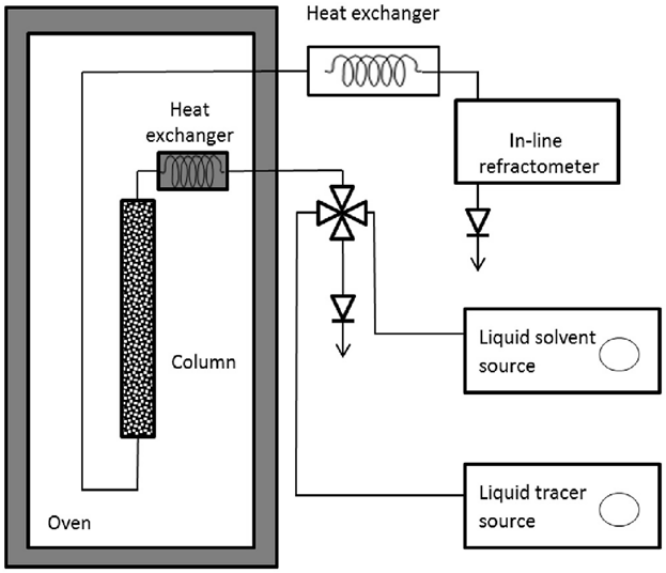

Figure 6: ILC experimental setup

A stainless steel column (50 cm in length and 1 cm in internal diameter) was filled with crushed and sieved particles and placed into an oven (all experiments were performed à 35°C). Solvent (heptane) was pumped into the column until the whole volume was filled and the temperature and pressure stabilized. At t=0, the liquid tracer (3 wt% squalane in n-heptane) was injected into the column. The response of the column to this step function (i.e. the breakthrough curve) was recorded using an online UR24 High Accuracy refractometer with absolute refractive index precision of 0.00007 nD. After the system reached equilibrium (i.e. the tracer concentration at the outlet of the column has reached the inlet concentration), pure solvent was injected in the column. Hence, for each experiment, both the positive steps (breakthrough curves) and the negative steps (inverse breakthrough curves, also called purge curves) were performed.

For each experiment, the first moment (mean residence time) μ_1 and the variance σ^2 of the breakthrough curve were evaluated and the HETP (Height Equivalent to a Theoretical Plate) calculated:

$$HEPT = \frac{\sigma^2}{\mu_1^2} L \tag{3}$$

The ILC experiments were interpreted using the well-known van Deemter equation[21]:

$$HEPT = A_1 + \frac{A_2}{v_i} + A_3 . v_i \tag{4}$$

with:

$$A_1 = 2\gamma_1 R_p \tag{5}$$

$$A_2 = 2\gamma_2 D_m \tag{6}$$

$$A_3 = \frac{R_p^2}{5 \cdot \varepsilon_p \cdot D_{eff}} \frac{2}{3} \frac{\left(\frac{1-\varepsilon_i}{\varepsilon_i}\right) . \varepsilon_p^2}{(1+\left(\frac{1-\varepsilon_i}{\varepsilon_i}\right) . \varepsilon_p)^2} \tag{7}$$

Eq. (7) is only valid if two assumptions are verified: adsorption at the pore surface is negligible and external resistance is not a limiting step for mass transfer. Preliminary experiments detailed in a previous paper[2] allowed to validate these hypotheses.

Parameter A_3 defined by eq. (7) is the slope of the Van Deemter curve and can be interpreted as the characteristic diffusion time of the molecules inside the porous particle. It can be determined experimentally by tracing the evolution of the HETP as a function of fluid interstitial velocity. The experimental characteristic diffusion time is not only dependent on tortuosity, but also on different structural parameters, such as the different levels of porosity ε_i and ε_p and particle radius. Hence, these parameters have to be evaluated with care, in order not to introduce a bias on the tortuosity factor value.

The tortuosity factor can be evaluated from equations (1) and (7):

$$\tau = \frac{A_3 5 \varepsilon_p D_m}{R_p^2} \cdot \frac{3}{2} \cdot \frac{(1+\left(\frac{1-\varepsilon_i}{\varepsilon_i}\right).\varepsilon_p)^2}{\left(\frac{1-\varepsilon_i}{\varepsilon_i}\right).\varepsilon_p^2} \qquad (8)$$

meaning that any imprecision on the latter variable will have a large impact on the tortuosity factor value.

Catalytic experiments

In order to assess the diffusion limitations under operating conditions representative of liquid-phase vacuum gas oil hydrotreating, a high-boiling (400°C < T_{eb} < 550°C, corresponding to a molecule with a carbon number between 25 and 45 carbon atoms), but very reactive sulphur-containing molecule is needed so as to observe competition between diffusion and chemical reaction. Such a sulphur-containing molecule, 2,5-*bis*-(octadecyl)thiophene ($C_{40}H_{76}S$), was synthesized according to an already described protocol[22].

1.7 g of thiophene and 10 mL of anhydrous tetrahydrofurane were introduced in a stirred vessel under argon at 195 K. *n*-BuLi (2.5 M in hexane; 25 mL, 2.5 equivalents) was added drop by drop. The mixture was then slowly warmed up to 293 K and stirred for 24 hours. The solution is then cooled down to 195 K and 1-bromootacdecane (13.8 g; 2.5 equivalents) was added. After 30 minutes of stirring, the vessel was again slowly warmed up to 293 K and stirred for 24 hours. The product was precipitated at 273 K, washed with cyclohexane and dried with $MgSO_4$. The solvent was removed under vacuum and yielded a yellowish solid. A total of 10 g of 2,5-*bis*-(octadecyl)thiophene was obtained with a purity of 93% (^{1}H NMR: δ_H (400 MHz, $CDCl_3$), 0.88 (6 H, t, 2 x CH_3), 1.29 (60 H, m, 30 x CH_2), 1.64 (4 H, m, 2 x CH_2), 2.72 (4H, t, 2 x CH_2) and 6.52 (2 H, s, C_4H_2S).

The catalytic experiments were performed in a three-phase semi-batch Robinson-Mahoney reactor at high temperature and pressure. The reactor vessel has a total volume of 500 mL. Pressure is kept constant by feeding hydrogen from an external gas tank that allows to monitor the hydrogen consumption. The reactor is also equipped with a high-pressure liquid injector (30 mL capacity) and a liquid-phase sampling line. The catalyst is maintained in a cylindrical basket, while the gas and liquid are intensely mixed by means of a Rushton stirrer rotating at 1200 rpm.

The catalysts (1 g) were sulphided prior to the experiment in a plug flow glass reactor as previously described.[22] The catalyst was loaded in the reaction vessel in a glove box with 176 g of squalane,

DMDS (3 g) and t-butylamine (0.9 g). The liquid prevents catalyst re-oxidation during the transfer from the glove box to the reactor. The reactor is initially flushed with nitrogen at 10 barg, followed by hydrogen flushing. 2.2 g of 2,5-*bis*-(octadecyl)thiophene in 20 g of squalane was introduced in the high-pressure liquid injector and the reactor was heated to the reaction temperature (613 K). At this temperature, the injector was emptied in the reactor and the total pressure was adjusted to 55 barg by means of the hydrogen supply from the external gas tank.

At the start of the reaction, the reaction mixture (250 mL of liquid at 293K) was therefore composed of $C_{40}H_{76}S$ (1 wt%), DMDS (1.5 wt%) and t-butylamine (0.5 wt%) dissolved in squalane (97 wt%) as solvent. DMDS and t-butylamine quickly decompose at 340°C with hydrogen to form H_2S and NH_3 respectively, which allows to simulate their partial pressures observed at the outlet of an industrial hydrotreating reactor. During the experiments, the liquid phase is sampled at regular intervals in order the measure the hydrodesulphurisation of 2,5-*bis*-(octadecyl)thiophene. Prior experiments were performed to ensure that the thermal conversion of the sulphided molecule is negligible (less than 1 wt% of conversion per hour). The thermal decomposition of squalane is also negligible (below 1 wt% at 613 K after 6 hours).

The catalytic experiments were interpreted using a model based on the following assumptions:

1. The reactor is isothermal and the extragranular fluid phase is homogeneous (perfectly mixed reactor).
2. The catalyst particles are spherical with an average radius R_p.
3. An external film resistance between the fluid and the particle surface is assumed. In practice, this resistance was assumed to be negligible in our experimental conditions. It was nevertheless kept in the model, for numerical considerations.
4. Mass transfer inside the particles is governed by Fickian diffusion inside the mesopores.
5. Reaction is of first order and takes place in the intragranular phase. The stoichiometric coefficient is -1 for the reactant.

Mass balances on the fluid phase and on the particles yield the following model equations:

- Mass balance on the fluid phase:

$$V_f \frac{\partial C_f(t)}{\partial t} = -S.k_L.\left(C_f(t) - C_p\left(t, r = R_p\right)\right) \quad (9)$$

- Mass balance on the particles:

$$\frac{\partial C_p(t,r)}{\partial t} = D_{eff}.\frac{1}{r^2}.\frac{\partial}{\partial r}\left(r^2.\frac{\partial C_p(t,r)}{\partial r}\right) - k_r.\frac{1-\varepsilon_p}{\varepsilon_p} C_p(t,r) \quad (10)$$

- Particle boundary conditions:

At r=0, $$\left.\frac{\partial C_p(t,r)}{\partial r}\right|_{r=0} = 0 \quad (11)$$

At $r=R_p$, $$S.k_L.\left(C_f(t) - C_p\left(t, r = R_p\right)\right) = S_{eff}.D_{eff}.\left.\frac{\partial C_p(t,r)}{\partial r}\right|_{r=R_p} \quad (12)$$

- Initial conditions:

A t=0, $$\mathrm{C_f(t=0) = C_{f0}} \quad (13)$$

A t=0, $$\forall \mathrm{r}, \mathrm{C}_p(\mathrm{t}=0, \mathrm{r}) = 0 \quad (14)$$

The solid particle is spatially discretized with centred finite difference method. Simulation of the model is performed with MATLAB using integration solver *ode23s*. Parameter estimation was carried out using the *lsqnonlin* algorithm. The objective function to be minimized was the sum of the squares of the error between the calculated and measured concentrations. Based on the assumption that the errors of estimation follow a normal distribution, the 95% normal confidence interval of the parameters was obtained.

Molecular diffusion

To estimate the particle tortuosity factor from effective diffusion measurements, molecular diffusion has to be independently evaluated (eq. (1)). For all experiments performed at low temperature (i.e. PFG-NMR and ILC), the molecular diffusion coefficients were measured using liquid-phase PFG-NMR and can be found in Table 6. However, since PFG-NMR is not practicable in our catalytic operating conditions (340°C and 56 bar), the Hayduk and Minhas correlation[23] was used instead. This correlation, specially developed for linear paraffin systems, predicted with excellent accuracy the molecular diffusion coefficients measured by PFG-NMR for our systems at lower temperature (Table 6).

		D_m (10^{-9} $m^2.s^{-1}$)	
Tracer-Solvent	Temperature (°C)	PFG-NMR ^1H	Hayduk and Minhas correlation [23]
SQ-nC7	35	1.6	1.6
$C_{40}H_{76}S$-SQ	35	0.064	0.062
$C_{40}H_{76}S$-SQ	340	-	3.5

Table 6: Molecular diffusion coefficients

Results and discussion

Tortuosity from NMR measurements

The tortuosity factors evaluated by PFG-NMR are listed in Table 7. The means square displacement of the molecules $< r(t) >$ varies between 24 and 34 µm, that is to say much smaller than the mean diameter of the particles (around 800 µm). The assumption of a negligible contribution of mass transfer between the mesopores and the liquid phase is therefore validated.

Sample	D_{eff} (10^{-9} $m^2.s^{-1}$)	τ	$< r(t) >$ (µm)
A	0.70	3.4	24
B	0.88	2.7	27
C	0.78	3.1	26
D	1.00	2.4	29
E	1.34	1.8	34

Table 7: PFG-NMR toluene diffusion results

Even though all the samples have very similar porosities (Table 2), their tortuosity factors vary by nearly a factor of two, meaning that the organization of the pore network plays a significant role in the diffusion process.

PFG-NMR vs. ILC experiments

The Van Deemter curves, shown on Figure 7, show the expected linear behaviour on the whole range of interstitial velocities for all samples. The HETPs range between 1 and 7 cm, meaning that the column (length 50 cm) comprises between 7 and 50 theoretical plates.

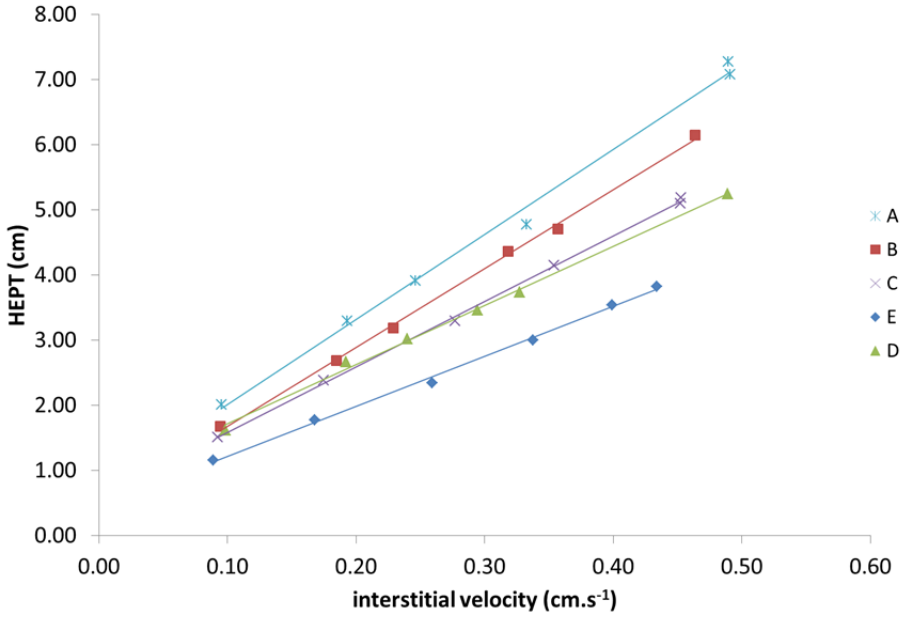

Figure 7: Van Deemter curves for all samples

The ILC tortuosity factors were estimated from the slope of the Van Deemter curves using eq. (8) and compared to the values obtained with PFG-NMR on Figure 8. As previously discussed, the value of the tortuosity factor calculated from the ILC experiments depends on the assumption for the mean particle radius calculation.

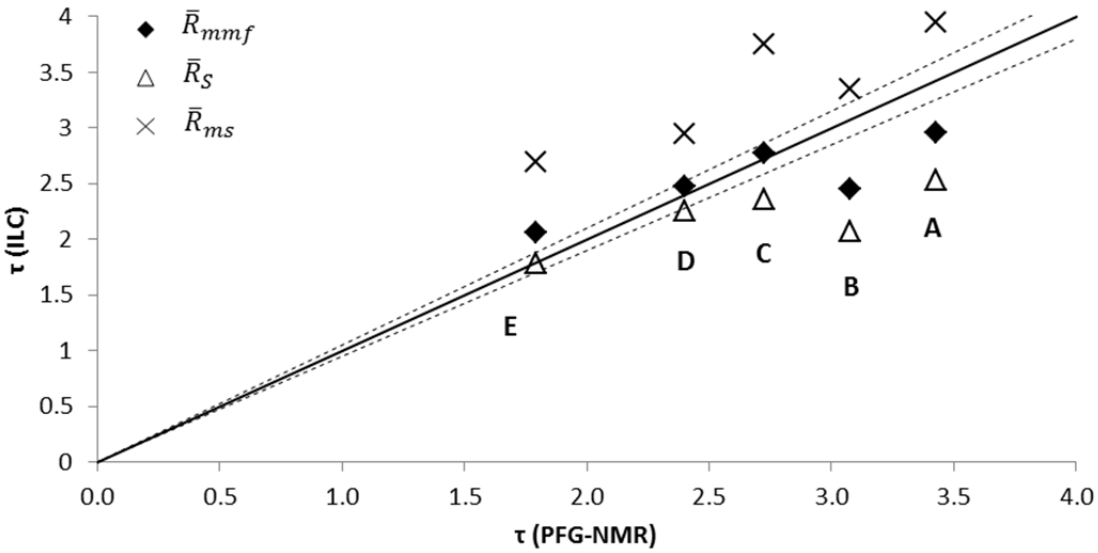

Figure 8: Tortuosity factors from ILC vs. PFG-NMR for different mean radii (as defined in Table 3). The dotted lines indicate a 5% error margin

The tortuosity factors from ILC experiments are mostly consistent with the values obtained by PFG-NMR: the different samples rank in the same order whatever the technique used, except for sample B. From Figure 8, it is also clear that the tortuosity factors obtained by ILC vary significantly depending on the expression used to calculate the mean particle radius. From the three possible mean radii, the Mean Molar Flux Radius $\bar{R}_{mmf}$, which is based on the hypothesis of a constant molar intraparticle flux density, yields the ILC tortuosity factors closest to those of PFG-NMR.

Tortuosity from catalytic experiments

In order to assess the effects of mass transfer and chemical kinetics on the conversion kinetic of the sulphur molecule, catalytic experiments were performed with particles of different sizes (Table 8).

Experiment n°	Support preparation	Radius (mm)
C1	As-synthesized trilobe extrudates manually sorted by length (4-5 mm)	R_S^{eq}=0.84 R_D^{eq}=1.14
C2	Crushed and sieved between 800 and 900 µm	$\bar{R}_{mmf}$=0.422
C3	Crushed and sieved between 800 and 900 µm	$\bar{R}_{mmf}$=0.422
C4	Crushed and sieved between 50 and 100 µm	$\bar{R}_{mmf}$=0.038

Table 8: Catalytic experiments conditions (support D, T=340°C, P= 56 bar)

The resulting concentration profiles vs. time are shown on Figure 9.

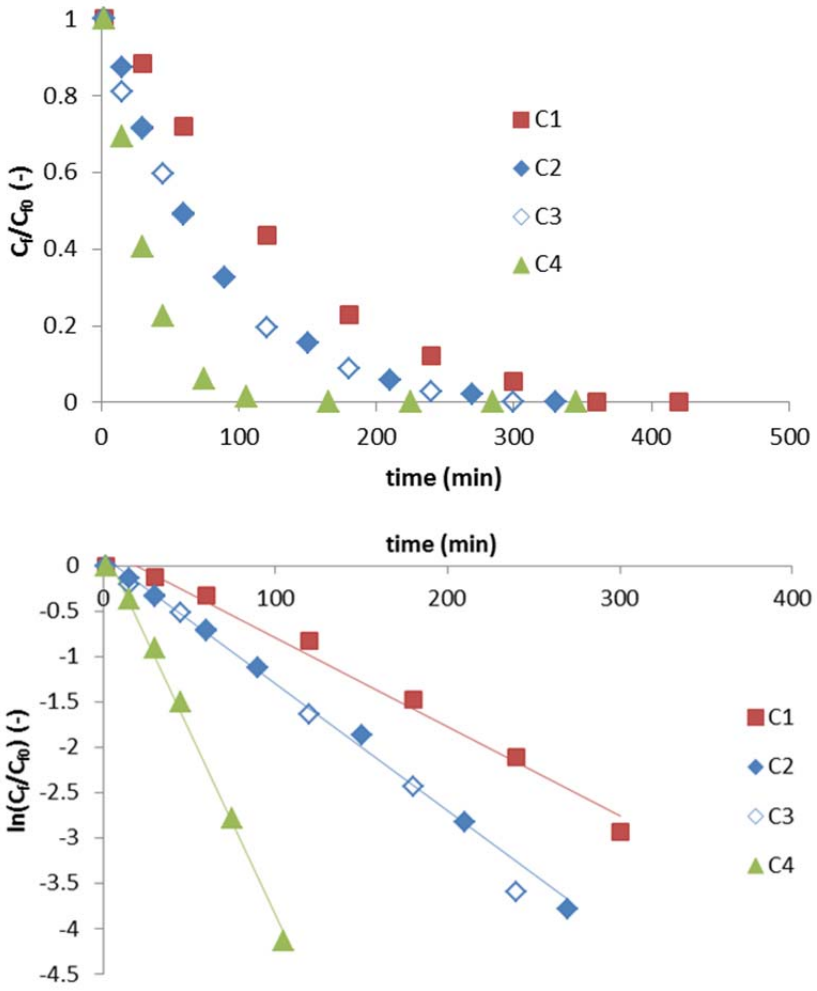

Figure 9: Concentration profiles of $C_{40}H_{76}S$ for the different shapes and sizes of the catalyst: (a) normalized concentration C/C_0 (b) ln(normalized concentration) vs. time

The agreement between experiments C2 and C3, carried out in the same conditions, demonstrates the good reproducibility of the experiments. Also, the effect of particle size is very clear: the smaller the particle, the faster the decrease in $C_{40}H_{76}S$ concentration. This suggests that internal mass transfer is the limiting the reactions rates, at least for the larger particles. Finally, $\ln(C/C_0)$ decreases linearly with time, confirming apparent first-order kinetics, which is what one should obtain for an internal-diffusion limited process[24].

The reaction rate constant and the particle tortuosity factor were estimated from experiments C2 to C4 (conducted with crushed particles) using eqs. (9) to (14). The estimated values are given in Table 9, together with the 95% confidence interval. To illustrate the quality of the regression, Figure 10 shows that the simulations exhibit a very good agreement with the experimental data for experiments C2 to C4.

	Catalytic reactor	ILC	PFG-NMR
Tortuosity factor τ (-)	2.09 ± 0.36	2.47	2.40
Rate constant k (s^{-1})	2.33 ± 0.2	-	-

Table 9: Estimated parameters for catalyst SCD (catalytic reactor) and initial support D (ILC and PFG-NMR experiments)

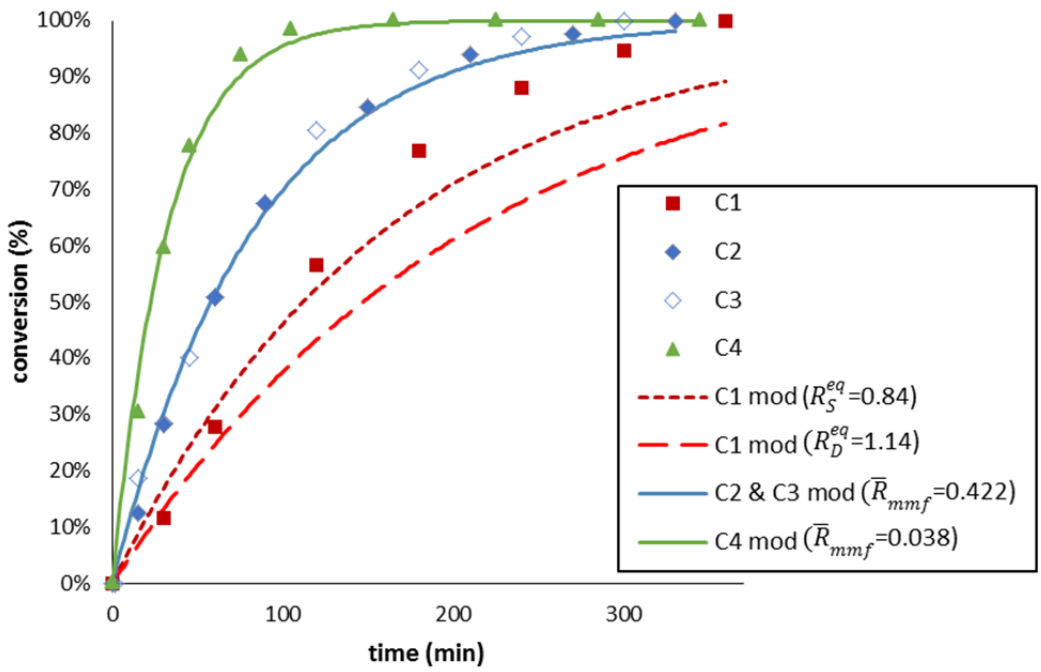

Figure 10: Experimental vs. simulated conversion for the catalytic experiments

As can be seen from Table 9, the tortuosity factor estimated from the catalytic experiments is in good agreement with those obtained by PFG-NMR and by ILC. This is even more remarkable given the very different experimental conditions used for each technique, as already mentioned in Table 1.

Using the parameters from Table 9, experiment C1 was simulated without any further tuning. As this experiment was made with as-synthesized (non-crushed) extrudate trilobes, a sphere-equivalent radius has to be calculated. The simulations obtained with the Sauter-equivalent radius R_S^{eq} and with the diffusion-equivalent radius R_D^{eq} are compared on Figure 10 (for the definitions of the sphere-equivalent radii, see the

Experiments and Methods section). Neither of the two sphere-equivalent radii yields an adequate fit of the experimental data: the short-time data are relatively well represented, but the simulations systematically underestimate the conversion at longer times. This suggests that the shape of the curve obtained with trilobes cannot be represented with a model assuming diffusion in spherical particles. Similar conclusions have been reached in previous simulation studies by comparing concentration profiles in batch[8] or fixed-bed[11] reactors for spheres, slabs and cylinders.

Nevertheless, the simulated curve obtained with the Sauter-equivalent radius R_S^{eq}, i.e. the radius that conserves the same external exchange surface, is closer to the experimental data, which might seem surprising for a supposedly diffusion-limited process. The simulated concentration profiles for the sulphur-compound inside the particles of different sizes, shown on Figure 11, explain these apparently inconsistent results.

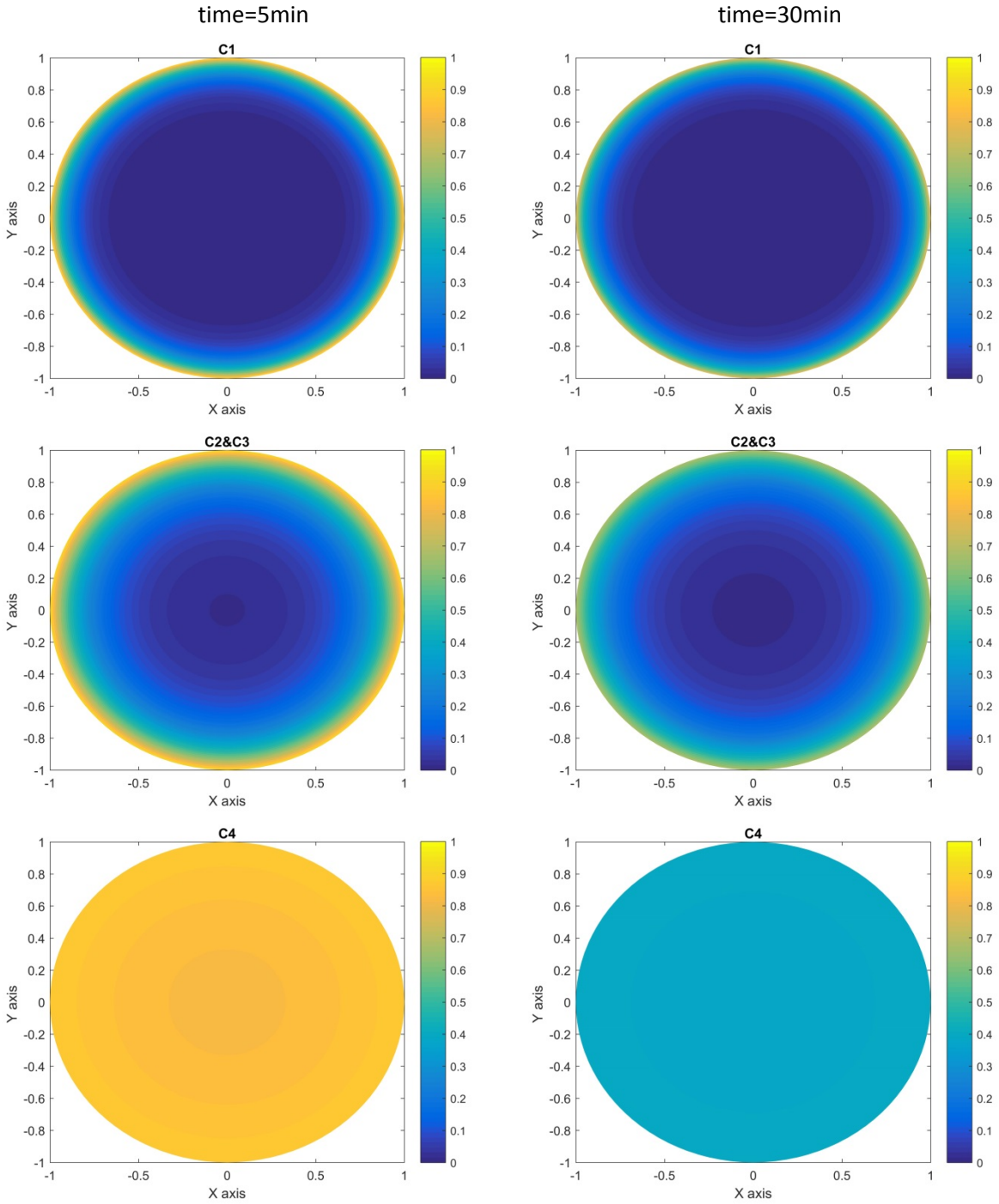

Figure 11: Simulated concentration profiles along the particle's normalized radius for the three particle sizes (C1: R_S^{eq}=0.84 mm; C2 and C3: $\overline{R}_{mmf}$=0.422 mm; C4: $\overline{R}_{mmf}$=0.038 mm)

For the smallest particles C4, the concentration profiles are almost flat, i.e. the conversion is limited by the reaction kinetics. On the contrary, for the largest particles C1, conversion is extremely diffusion-rate limited: the concentration drops very fast, to such an extent that only the external part of the particle is actually "explored" by the sulphur-compound. As the concentration gradient is very strong and nearly limited to the external surface of the particle, the overall rate of disappearance is

close to that of a surface diffusion-limited system. This explains why the Sauter-equivalent radius is more adequate in that particular case.

More generally, it can be concluded from these catalytic experiments that the effects of the particle shape on the overall reaction rates are far from negligible. Modelling reactions in trilobe extrudates using an equivalent sphere assumption may lead to important misinterpretation: not only are the forms of the curves different, but also the equivalent radius depends on the rate-limiting phenomena.

Conclusions and perspectives

The mass transfer properties of hydrotreating catalyst supports was evaluated using PFG-NMR, ILC and catalytic experiments. By comparing ILC and PFG-NMR results, a new expression was proposed to evaluate the mean radius of the catalyst particles, needed to evaluate the tortuosity factor from ILC experiments. A wide range of tortuosity factors was obtained: even though the supports have similar porosities (around 0.7 mL/mL), the tortuosity factors range from 1.8 to 3.4, which can probably be explained by the complex multiscale organization of the γ-alumina pore network. One support was impregnated with NiMoP and sulphided, and the resulting catalyst was tested in a batch reactor for the hydrodesulphurization of 2,5-bis-(octadecyl)thiophene ($C_{40}H_{76}S$), a reactive sulphur-compound boiling in the Vacuum Gas Oil range. By performing catalytic experiments with different particle sizes, the intrinsic reaction rate parameter and the catalyst tortuosity factors were estimated. Given the experimental uncertainties, the tortuosity factor of the catalyst is close to that of the support, showing that the impregnated and sulphided oxide layer does not modify substantially the mass transfer properties of the support. These results also show that a support tortuosity factor can be extrapolated from non-reactive microscopic (NMR) or macroscopic (ILC) techniques to reactive conditions, provided that the experimental results are properly interpreted.

In this respect, this work demonstrates that the particle shape factor and the particle size distribution play a significant role in the mass transfer behaviour of catalyst supports and have therefore to be taken into account. To simplify, the existing models suppose spherical and uniformly sized particles. It is therefore necessary to correctly calculate the equivalent and/or mean particle radii, whose value depends on the overall rate limiting step (intraparticle diffusion, surface diffusion or chemical reaction). When the chemical reaction is very fast compared to diffusion (high Thiele modulus) or when surface diffusion is the limiting step, it is recommended to use the Sauter radius, which conserves the same surface to volume ratio of the catalyst. When intraparticle diffusion is the limiting step, the new mean radius introduced in this work - the mean molar flux radius – yields better results.

Nonetheless, the conversion vs. time curve of the trilobe pellet catalyst cannot be accurately represented by a sphere-equivalent model. In order to precisely simulate and optimize the performances of industrial catalysts, which are commonly shaped as trilobes or quadrilobes, a more accurate representation of the catalyst shape is needed, which implies the use of complex mathematical simulation tools.

Notations

C_f: Fluid phase concentration (mol.m^{-3})

C_{f0}: Initial fluid phase concentration (mol.m^{-3})

C_p: Concentration in the particle mesoporosity (mol.m^{-3})

$\bar{C}_{i,p}$: Mean concentration in the particle mesoporosity (mol.m^{-3})

D_{eff}: Effective diffusivity (m^2.s^{-1})

D_m: Molecular diffusivity (m^2.s^{-1})

ε_i: Interstitial porosity (-)

ε_p: Particle porosity (-)

γ_1, γ_2: Constants in equations 5 and 6 (-)

$HETP$: Height Equivalent of a Theoretical Plate (m)

k_L: External fluid film mass transfer coefficient (m.s^{-1})

k_r: Chemical kinetic constant (s^{-1})

L: Column length (m)

L_p: pellet length (m)

μ_1: First order moment (s)

r: Radial coordinate (m)

R_p: Particle radius (m)

ρ_s: Structural density measured by helium pycnometry (g.cm^{-3})

σ^2: Centered second moment (s^2)

S: External surface of the catalyst particles (m^2)

S_{eff}: Effective surface of the catalyst particles ($S_{eff} = S \cdot \varepsilon_p$ (m^2)

S_{BET}: BET surface (m^2.g^{-1})

τ: Tortuosity factor (-)

v_i: Interstitial velocity of fluid (m.s^{-1})

V_p: Pore volume of the particle (cm^3.g^{-1})

V_f: Fluid volume in the reactor (m^3)

V_R: Reactor volume (m^3)

n_T: Total number of particle in the reactor volume (-)

$x_i(R_i)$: Number fraction of particles with radius R_{pi} (-)

$\bar{R}_S$: Mean Sauter radius (m)

$\bar{R}_{ms}$: Mean square radius (m)

$\bar{R}_{mmf}$: Mean molar flux radius (m)

R_{lobe}: Radius of the lobe (m)

R_S^{eq}: Sauter-equivalent radius (m)

R_D^{eq}: Diffusion-equivalent radius (m)

R_{cyl}^{eq}: Cylinder-equivalent radius (m)

J: Molar flux at the surface of the particles ($mol.m^{-2}.s^{-1}$)

$\bar{J}$: Mean molar flux at the surface of the particles ($mol.m^{-2}.s^{-1}$)

References

[1] H. Toulhoat, P. Raybaud, "Catalysis by Transition Metal Sulphides: from Molecular Theory to Industrial Application", Editions Technip, Paris, **2013**.

[2] S. Kolitcheff, E. Jolimaitre, A. Hugon, J.J. Verstraete, P.-L. Carrette, M. Tayakout-Fayolle, "Tortuosity of mesoporous alumina catalyst supports: Influence of the pore network organization", *Microporous and Mesoporous Materials*, **2017**, 248, 91-98.

[3] L. Shen, Z. Chen, "Critical review of the impact of tortuosity on diffusion", *Chemical Engineering Science*, **2007**, 62(14), 3748–3755.

[4] S.M. Auerbach, K.A. Carrado, P.K. Dutta, "Handbook of zeolite science and technology", M. Dekker, New York, **2003**.

[5] D.M. Ruthven, K.F. Loughlin, "The effect of crystallite shape and size distribution on diffusion measurements in molecular sieves", *Chemical Engineering Science*, **1971**, 26(5), 577–584.

[6] A.S. Moharir, D. Kunzru, D.N. Saraf, "Theoretical prediction of sorption curves for molecular sieves", *Chemical Engineering Science*, **1980**, 35(6), 1435–1441.

[7] G. Carta, A. Ubiera, "Particle-size distribution effects in batch adsorption", *AIChE J.*, **2003**, 49(12), 3066–3073.

[8] H. Başağaoğlu, B.J. McCoy, T.R. Ginn, F.J. Loge, J.P. Dietrich, "A diffusion limited sorption kinetics model with polydispersed particles of distinct sizes and shapes", *Advances in Water Resources*, **2002**, 25(7), 755–772.

[9] A.S. Moharir, D. Kunzru, D.N. Saraf, “Effect of adsorbent particle size distribution on breakthrough curves for molecular sieve columns”, *Chemical Engineering Science*, **1980**, 35(8), 1795–1801.

[10] A. Rasmuson, “The effect of particles of variable size, shape and properties on the dynamics of fixed beds”, *Chemical Engineering Science*, **1985**, 40(4), 621–629.

[11] A. Rasmuson, “Modeling of solute transport in aggregated/fractured media including diffusion into the bulk matrix”, *Geoderma*, **1986**, 38(1-4), 41–60.

[12] F.K. Fong, L.A. Mulkey, “Comparison of numerical schemes for solving a spherical particle diffusion equation”, *Water Resources Research*, **1990**, 26(5), 1291–1303.

[13] C. Hayot, F. Lafolie, “One-dimensional solute transport modelling in aggregated porous media. Part 2. Effects of aggregate size distribution”, *Journal of Hydrology*, **1993**, 143(1-2), 85–107.

[14] A.S. Moharir, D. Kunzru, D.N. Saraf, “Modelling of nonisothermal packed bed sorption on uniform and nonuniform zeolite crystals”, *Zeolites*, **1982**, 2(3), 155–161.

[15] G. Carta, J.S. Bauer, “Analytic Solution for Chromatography with Nonuniform Sorbent Particles”, *AIChE J.*, **1990**, 36(1), 147–150.

[16] J. Ancheyta, J. Muñoz, M.J. Macías, “Experimental and theoretical determination of the particle size of hydrotreating catalysts of different shapes”, *Catalysis Today*, **2005**, 109(1-4), 120–127.

[17] R. Mesnier, “Étude des liens entre la texture et les propriétés de diffusion de molécules modèles dans des milieu poreux bimodaux”, Ph.D. thesis, Institut National Polytechnique de Toulouse, **2008**.

[18] M.T. van Genuchten, “A general approach for modeling solute transport in structured soils”, Memoires Int. Assoc. Hydrogeol., **1985**, 17, 513–526.

[19] H. Wang, F. Willot, M. Moreaud, M. Rivallan, L. Sorbier, D. Jeulin, “Numerical Simulation of Hindered Diffusion in γ-Alumina Catalyst Supports”, *Oil Gas Sci. Technol. – Rev. IFP Energies nouvelles*, **2017**, 72(2), 8.

[20] https://www.bruker.com/products/mr/nmr/nmr-software/nmr-software/dynamics-center/overview.html

[21] D.M. Ruthven, “Principles of adsorption and adsorption processes”, Wiley, New York, **1984**.

[22] J.C. Swarts, E.H.G. Langner, N. Krokeide-Howe, M.J. Cook, J. Mater. Chem. 2001, 11, 434

[23] W. Hayduk, B.S. Minhas, “Correlations for prediction of molecular diffusivities in liquids”, *Can. J. Chem. Eng.*, **1982**, 60(2), 295–299.

[24] M.E. Davis, R.J. Davis, “Fundamentals of chemical reaction engineering”, McGraw-Hill, Boston, **2003**.